NATIONAL UNIVERSITY OF SCIENCE AND TECHNOLOGY POLITEHNICA BUCHAREST

DOCTORAL SCHOOL OF ELECTRICAL ENGINEERING

DOCTORAL THESIS

-SUMMARY-

CONTRIBUTIONS TO THE POWER SUPPLY OF SURFACE DRONES USING MOBILE MODULES WITH RENEWABLE ENERGY SOURCES

Scientific coordinator:
Prof.univ.dr.ing. Mihai Octavian POPESCU

PhD student:
Eng. Nicolae-Silviu POPA

BUCHAREST
2025

CONTAINED

CHAPTER 1. INTRODUCTION

Surface drones have evolved significantly due to intense research and interest from economic, political, and military fields. The first surface drone, introduced by Nikola Tesla in 1898, was a radiowave-controlled vehicle, marking a major advance in robotics and autonomous technology. [1], [2]

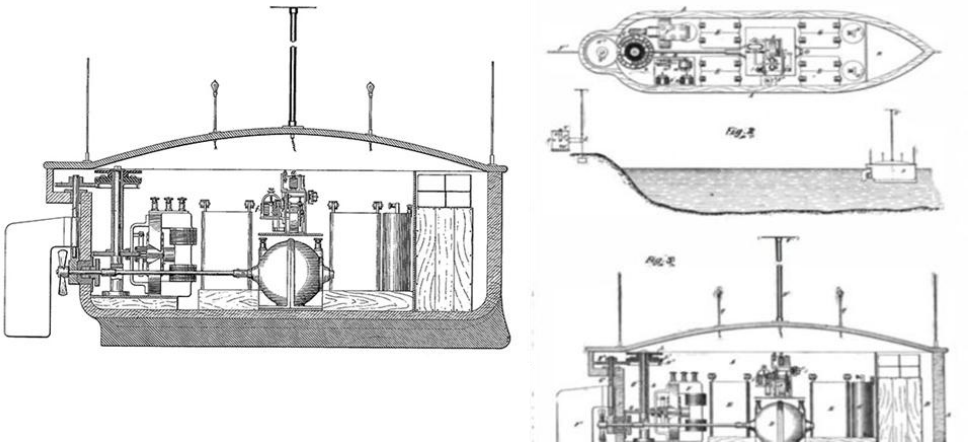

Figure 1.1 – The first remote-controlled drone/surface platform [2]

Surface drones, also known as USVs (Unmanned Surface Vehicles), are autonomous craft used in various fields such as hydrography, oceanography, ecology, surveying, and military. They have advanced tactical and technical characteristics, such as a small displacement, high speed, and a low radar and sound footprint, which give them invisibility on radars and sonars. These drones are constantly connected to a command center that assigns them specific missions and tasks. [3], [4], [5], [6], [7]

Mobile systems with renewable sources are designed to power surface drones, being characterized by mobility, reduced assembly time and energy independence. These systems use adjustable photovoltaic panels to maximize electrical production and can be used in various environments, having both civil and military applications. [8], [9], [10], [11], [12]

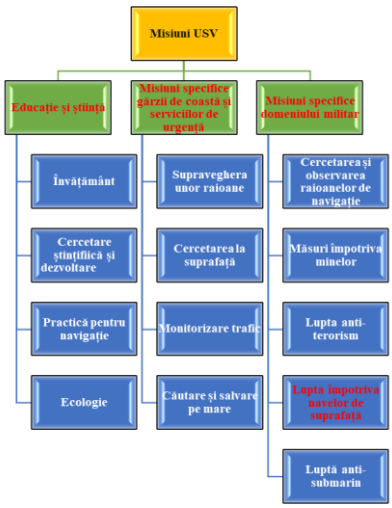

Figure 1.2 – Missions that can be executed by surface drones

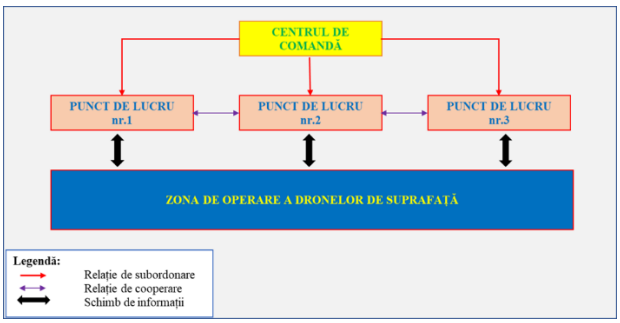

Figure 1.3 – Organizational chart of the execution of surface drone missions

The renewable energy supply of surface drones offers sustainable and energy-independent solutions, essential in the current geopolitical context. The mobile modules allow operation in isolated locations and can serve as a backup for ships' communication and navigation systems.

1.1. THEME OBJECTIVES

Since mobile modules for powering surface drones with renewable energy are mounted on water, a main objective is to develop a mathematical model for determining the albedo according to hydrometeorological parameters. It optimizes the use of photovoltaic systems and surface drones. Another objective is the study of photovoltaic systems for powering drones in maritime or river areas to increase the efficiency of battery charging. A third objective is to analyze the influences of the marine environment on electricity production, mathematical modeling, simulation, data acquisition and validation. The thesis aims to make practical devices and a demonstrator for the production of electricity using mobile modules with renewable sources. It also aims to disseminate the results by publishing in scientific articles and participating in international conferences.

CHAPTER 2. CURRENT STATE OF SUPPLY OF SURFACE DRONES VIA MOBILE MODULES

2.1.RENEWABLE ENERGY SOURCES TO POWER SURFACE DRONES

2.1.1. Solar energy and photovoltaic systems

The photovoltaic cell is similar to the p–n junction used in diodes and many semiconductor devices. Many types of semiconductor materials are used to create a photovoltaic cell, but silicon is currently the most common. Silicon dioxide is very abundant, making up more than half of the earth's crust. However, the pure silicon needed to create efficient cells is very energy-intensive. [17], [18]

The two elements of the photovoltaic cell form the static *PN* junction , leaving a positive charge on one side and a negative charge on the other side. When a photon of sunlight hits the photovoltaic cell, with enough energy, the electrons begin moving on the negative side of the *PN junction*. [16], [17], [19]

Surface drones, powered by renewable energy, are used in hydrography, oceanography, ecology, surveying, and military. They have advanced features and are connected to a command center. Adjustable photovoltaic modules, used to power drones, provide mobility and energy independence. [12], [13], [14]

In the production of electricity using photovoltaic panels, we must take into account Albedo. **Albedo** is a measure of the reflection or ability of a surface to reflect solar radiation. It is expressed as a ratio between the radiation reflected by a surface and the radiation incident on that surface, with values between 0 and 1. [20], [21], [22]

In the data provided by Transelectrica, significant differences are observed in the production of electricity through photovoltaic panels between July and December, caused by weather conditions. In July, the average production was approx. 500MW, and in December approx. 250MW, reflecting the duration of sunlight and the degree of cloudiness.

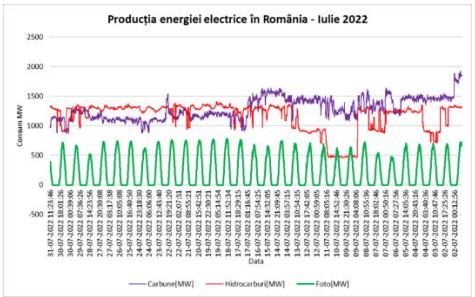

Figure 2.1 – Electricity production in July – 2022 [23]

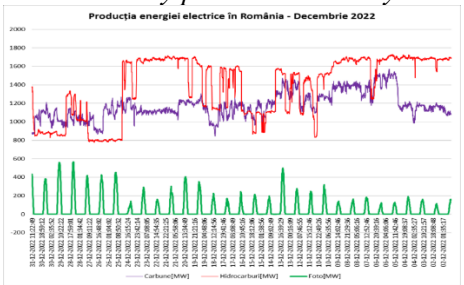

Figure 2.2 – Electricity production in December – 2022 [23]

2.2.ELECTRICITY STORAGE

2.2.1. Lithium batteries

Li-ion batteries are rechargeable, consisting of a lithium cathode, a graphite anode, and an electrolyte. They have long life cycles, sometimes exceeding 1000 cycles if used according to the manufacturer's specifications. There are various models and types of Li-ion batteries, each with its own characteristics and applications. [24], [25], [26]

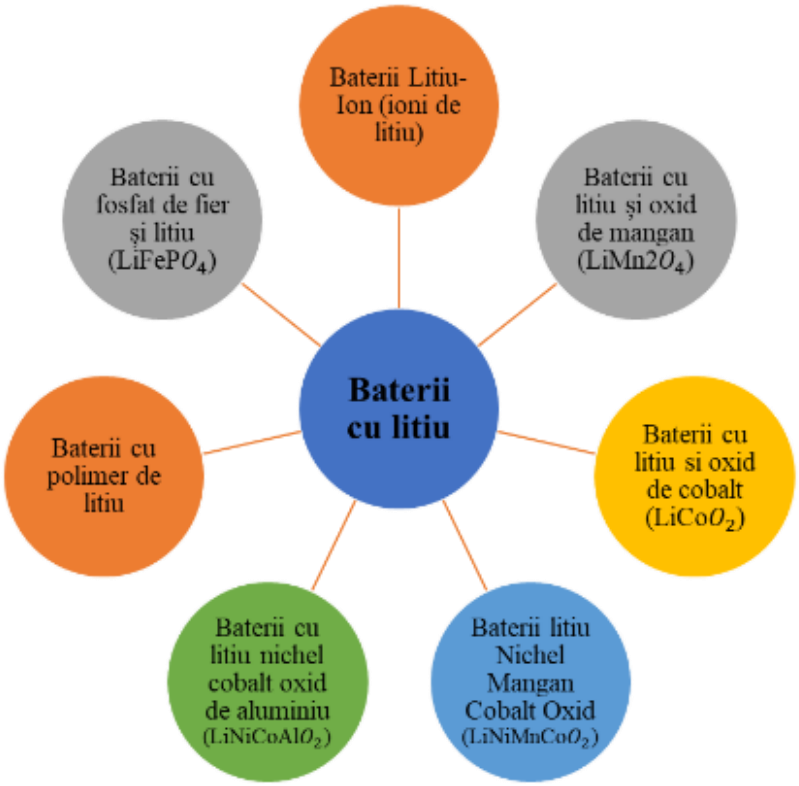

Figure 2.3 – Types of lithium-based batteries [27]

2.3.CONCLUSIONS AND PERSPECTIVES

Chapter 2 of the thesis discusses the use of surface drones powered by renewable energy in various fields and their advantages. The importance of these drones in civil and military operations, including research, border monitoring and the engagement of hostile surface ships, is underlined. The efficiency of Li-ion batteries and the importance of modeling photovoltaic systems for optimizing energy production are also mentioned.

CHAPTER 3. NUMERICAL MODELING OF PHOTOVOLTAIC SYSTEMS

3.1. GENERAL CONSIDERATIONS

The photovoltaic phenomenon produces a potential difference at the junction between two materials under solar radiation, similar to the photoelectric effect explained by Einstein in 1905. The energy of a photon is determined by the Planck constant, the frequency of the photon, the wavelength, and the speed of light.

$$E = h \cdot v = h \cdot \frac{c}{\lambda} \tag{3.1}$$

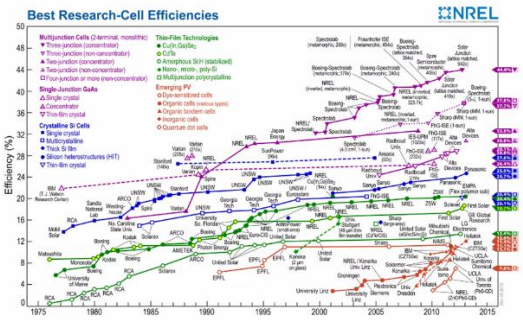

Figure 3.1. – The efficiency of the most important photovoltaic cell technologies [28]

3.2.PHOTOVOLTAIC CELL

3.2.1. I-V characteristic of photovoltaic cell.

The photovoltaic cell converts the energy received from the sun into electrical energy (direct current), which it *transfers to* an electrical circuit. In figure 3.3 we have shown the current-voltage characteristic of a photovoltaic cell. This figure will be the basis of future analysis and discussions.

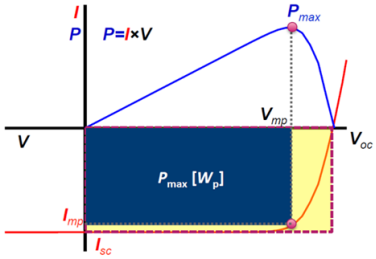

Figure 3.2 – I-V characteristic of a photovoltaic cell

The efficiency of the photovoltaic cell being given by the relationship 3.4

$$\eta = \frac{P_{max}}{P_I} = \frac{V_{mp} I_{mp}}{P_I} = \frac{V_{oc} I_{sc} FF}{P_I} \tag{3.2}$$

3.2.2. Photovoltaic cell construction

Photovoltaic cells convert solar energy into electricity. There are two main models of photovoltaic cells: the single-diode cell and the two-diode cell. The single-diode cell uses the Schottky diode to prevent energy loss in low light conditions. It improves the efficiency and performance of the cell by controlling the direction of the current and preventing damage to the system. Mathematical relationships describe how the current generated by the photovoltaic cell depends on the applied voltage, the specific parameters of the diode, temperature and lighting. [13], [29], [30], [31]

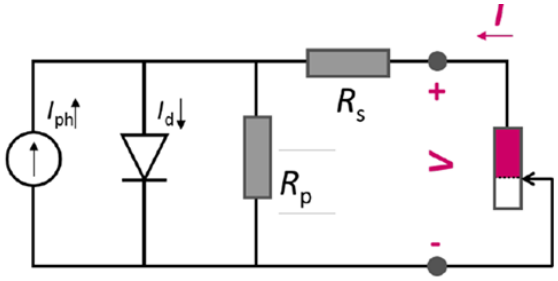

Figure 3.3 – Single-diode photovoltaic cell

$$I = I_0\left(e^{\frac{q(V-I\cdot R_S)}{n\cdot k_B\cdot T}} - 1\right) + \frac{V-I\cdot R_s}{R_p} - I_{ph} \tag{3.3}$$

Figure 3.4 shows the model of the photovoltaic cell with two diodes. The reason for this model is that there are two sources of current absorption in a photovoltaic cell and they must be modeled separately. Diode 1 represents the dark diffusion current. This diode has an ideality factor of 1, and diode 2 represents the dark recombination current and will have an ideality factor greater than 1. Many times, the ideality factor for diode 2 has a value of 2.

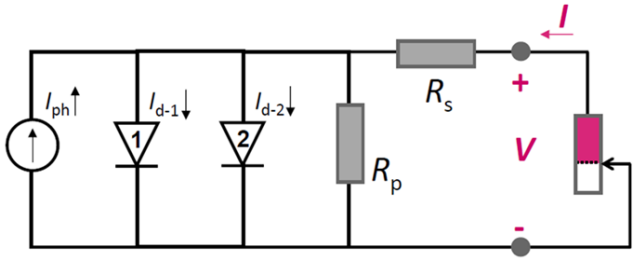

Figure 3.4 – Block diagram of a two-diode photovoltaic cell

Two-diode photovoltaic cells are advanced designs used to improve accuracy in simulating the behavior of solar cells under different lighting and temperature conditions. These models add an extra diode and resistor, making the current-voltage equation more complex, but providing more accurate predictions of the performance of photovoltaic cells. [13], [30], [32], [33], [34]

$$I = I_{01}\left(e^{\frac{q(V-I\cdot R_S)}{n_1\cdot k_B\cdot T}} - 1\right) + I_{02}\left(e^{\frac{q(V-I\cdot R_S)}{n_2\cdot k_B\cdot T}} - 1\right) + \frac{V-I\cdot R_s}{R_p} - I_{ph} \tag{3.4}$$

3.3. SIMULATION IN PVSYST OF MOBILE MODULES FOR POWERING SURFACE DRONES WITH RENEWABLE ENERGY SOURCES

3.3.1. Battery Packs

We cannot talk about the power supply of surface drones without mentioning battery packs and their characteristics. This section deals with important aspects for battery packs. The related information and graphs were obtained by generating them in the dedicated PvSist program. [35]

Battery packs are fundamental components in the context of drones and many other portable electronic devices. These stored energy sources ensure operation and mobility without the need for a constant power supply, such as a diesel generator. An important feature that influences the operationalization of the surface drone is the *Battery Capacity*.

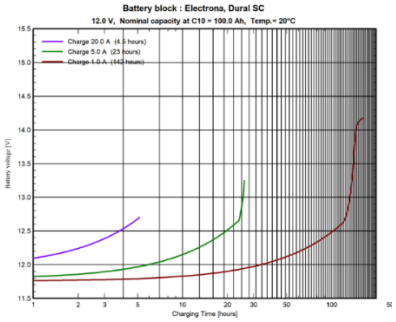

*Figure 3.6 – Charging characteristic of a battery with batteries: Nominal voltage 12 V; Operating temperature*20℃*; Batterylevel 100 Ah; purple is the battery charge characteristic at a current of 20 A (charging time 4.5 hours); green is the battery charging characteristic – current of 5A (charging time 23 hours); brown is the battery charging characteristic at a current of 1A (charging time 142 hours)*

Figure 3.7 shows the discharge characteristic, for three different current values, for the same battery model generated by PvSyst. Like the charging feature, the discharge feature of a battery pack should be considered when purchasing the battery.

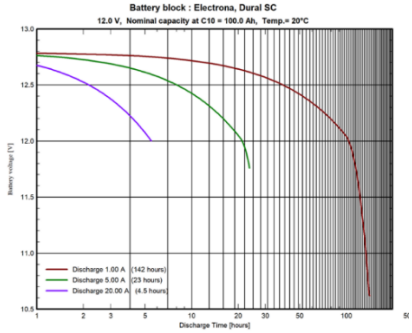

Figure 3.7 – Battery discharge feature.

From the two graphs it can be seen that the charging time of a battery with batteries is equal to the charging time, if the value of the charging current is equal to the value of the discharge current.

3.3.2. PvSyst Program

Battery packs are essential for surface drones, ensuring mobility without constant power supplies.

$$T_H = T_{Fas} \cdot T_{Diff} \quad (3.5)$$

The Perez Model is a more complex method of transposition compared to the Hay Model within PvSyst. This model involves a detailed analysis of diffuse irradiation and the factors that contribute to it. [36], [37]

The calculation of the transposition in this model () is given by the following mathematical relation:T_{Prez}

$$T_{Prez} = T_{Fas} \cdot T_{Diff} \cdot T_{Hor} \quad (3.6)$$

T_{Hor} – represents the specific transposition for horizontal measurements in the Perez model.

Transposition is calculated separately for each component of irradiation. The fascicular component assumes a purely geometric (cosine) transposition, which is not based on any physical model.

The beam component results from a purely geometric transposition:

$$Beam_{Inc} = \frac{Beam_{Hor} sin H_{soli}}{H_{sol}} \quad (3.7)$$

$$Diss_{Inc} = Diff_{Hor}[\frac{(1-K_B)(1+cosi)}{2} + K_B \sin(\frac{H_{soli}}{H_{sol}}) \ ] \quad (3.8)$$

The reflected radiation that reaches a collector plane, as mentioned above, is called Albedou:

$$Alb_{Inc} = \rho \cdot Glob_{Hor} \cdot \frac{1-\cos i}{2} \quad (3.9)$$

We can define the KB index as follows:

$$K_B = \frac{Beam_{Hor}}{I_0} \cdot \sin H_{sol} \quad (3.10)$$

$$I = I_{ph} - I_0\left(e^{\frac{q(V+I\cdot R_S)}{N_{cs}\cdot\gamma\cdot k_B\cdot T}} - 1\right) - \frac{V+I\cdot R_S}{R_p} \quad (3.11)$$

The photocurrent I_{ph} in a photovoltaic system varies depending on radiation and temperature and can be determined based on the reference values of solar radiation and temperature.

$$I_{ph} = I_{ph,ref} \cdot \frac{G}{G_{ref}} \cdot \left[1 + \beta_{I_{ph}} \cdot (T - T_{ref})\right] \quad (3.12)$$

PvSyst also operates the following mathematical models, in order to obtain as much clarity as possible on the simulated data:

a. The inverse saturation current of a diode (photovoltaic cells in our case), depending on the temperature:

$$I_0 = I_{0\,ref} \cdot \frac{T}{T_{ref}} \cdot 3 \cdot e^{\frac{q\cdot E_{Gap}}{\gamma\cdot K_B}\cdot\left(\frac{1}{T_{ref}} - \frac{1}{T}\right)} \quad (3.13)$$

b. The open-circuit voltage of a solar cell is derived from the Shockley equation, which models the behavior of the diode in a solar cell.

$$V_{OC} = \frac{nK_BT}{q} \ln(\frac{J_{PH}}{J_0} + 1) \quad (3.14)$$

c. The short-circuit current in a photovoltaic cell and is expressed as the integral of the product of the incident solar spectrum (ΦAM1.5(λ)), the quantum efficiency of the cell (EQE(λ)), and the elementary charge (q).

$$J_{sc} = q\int_o^{\lambda} \Phi_{AM1.5}(\lambda) EQE(\lambda) d\lambda \quad (3.15)$$

Thus, the mathematical model described by equation 3.42 can be simplified, obtaining the equation:

$$I = I_{ph} - I_0(e^{\frac{qV}{nkT}} - 1) \quad (3.16)$$

CHAPTER 4. SIMULATING THE OPERATION OF A PHOTOVOLTAIC CELL AT ALBEDO VARIATIONS IN LabVIEW

4.1.BASIC MATHEMATICAL MODELS IN THE OPERATION OF A PHOTOVOLTAIC CELL

The generation of electricity through photovoltaic panels involves complex mathematical models to optimize performance. Simulating the operation of albedo variations in LabView uses equations from the literature and experimental measurements. Equations 4.1 and 4.2 show the relationships of the current at the terminals of the panel and the photogenerated current.

$$I = I_{ph} - I_0\left(e^{\frac{q(V-I\cdot R_S)}{N_{CS}\cdot k_B\cdot T}} - 1\right) - \frac{V-I\cdot R_S}{R_p} \tag{4.1}$$

$$I_{ph} = I_{ph,ref}\cdot\frac{G}{G_{ref}}\cdot\left[1+\beta_{I_{ph}}\cdot\left(T-T_{ref}\right)\right] \tag{4.2}$$

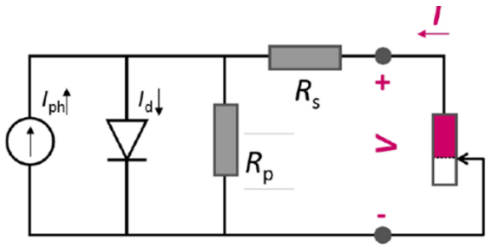

Figure 4.1 – Single-diode photovoltaic cell

The voltage at the terminals of the photovoltaic panel depends on the characteristics of the materials used and can be expressed by the equation:

$$V = N_c\cdot V_c = N_c\cdot\left(n\cdot V_T\cdot\ln\left(\frac{I+I_0}{I_0}\right)\right) \tag{4.3}$$

Where V represents the voltage at the terminals of the photovoltaic panel, N_c, V_c represents the number of photovoltaic cells connected in series, respectively the voltage of a single cell, represents the value of the thermal voltage.V_T

The photogenerated current equation (4.2) can be written as follows:

$$I_{ph} = \left(I_{sc} + K_i\cdot\left(T-T_{ref}\right)\right)\cdot\frac{S+S\cdot Alb\,(1-\cos\theta)}{S_{ref}} \tag{4.4}$$

Relationship 4.4 has the advantage of integrating several factors influencing electricity production and offers a way to more accurately model photovoltaic performance, which is important in stages such as: design, optimization and efficient management of solar energy systems. A simpler form of this equation is presented as equation 4.5.

$$I = I_{ph} - I_0(e^{\frac{qV}{nkT}} - 1) \tag{4.5}$$

Combining the current equation, known as the 4.1 relationship, with the photogenerated current equation, called the 4.4 relationship, yields a more complex formulation, called the 4.6 relationship, which describes the behavior of the current in detail. By substituting the photogenerated current equation, i.e. the 4.4 relation, into the 4.5 relation, a new equation is obtained, known as the 4.7 relation.

$$I = \left(I_{sc} + K_i\cdot\left(T-T_{ref}\right)\right)\cdot\frac{S+S\cdot Alb\,(1-\cos\theta)}{S_{ref}} - I_0\left(e^{\frac{q(V-I\cdot R_S)}{n\cdot k\cdot T}} - 1\right) - \frac{V-I\cdot R_S}{R_p} \tag{4.6}$$

$$I = \left(I_{sc} + K_i\cdot\left(T-T_{ref}\right)\right)\cdot\frac{S+S\cdot Alb\,(1-\cos\theta)}{S_{ref}} - I_0\left(e^{\frac{qV}{n\cdot k\cdot T}} - 1\right) \tag{4.7}$$

$$I_{ph} = (S + S\cdot Alb)\cdot\frac{A\cdot\eta}{S_{ref}} \tag{4.8}$$

$$I_{ph} = S \cdot A \cdot \eta \quad (4.9)$$

In order to estimate the photogenerated current more precisely, the efficiency of photovoltaic cells at different wavelengths and the contribution of radiation reflected by neighboring surfaces (albedo) are taken into account. The spectral weighted model with the spectral response function of the cell provides a more accurate assessment of the current generated. [38], [39], [40], [41], [42], [43]

$$I_{ph} = \int_{\lambda_{min}}^{\lambda_{max}} \Big(\big(S_\lambda \cdot SRF(\lambda) + S_\lambda \cdot Alb \cdot SRF(\lambda) \big) \cdot \eta \cdot A \Big) d\lambda \quad (4.10)$$

Equation 4.11 is a mathematical model of the dependence of the photogenerated current on the value of the albedo and the efficiency as a function of temperature of the photovoltaic cell.

$$I_{ph} = (S_{dir} + Alb \cdot G_{dir}) \cdot \eta(T) \cdot A \quad (4.11)$$

In the literature, we find an alternative formula for the photogenerated current (equation 4.12), which is determined by variables such as albedo, the efficiency of the photovoltaic panel, its surface, the temperature coefficient and the temperature at which the photovoltaic panel operates.(K_i)

$$I_{ph} = (S + S \cdot Alb) \cdot \eta \cdot A_{pv} + K_i \cdot (T_{Pv} - T_{ref}) \quad (4.12)$$

To derive the equations of the electricity generated by a photovoltaic system, we will substitute the value of the photogenerated current, described in the previous equations, in the simplified form of the current equation, known as the 4.5 relationship. This approach will allow us to formulate the following mathematical models:

- Substituting the value of the photogenerated current from the 4.8 relation to the 4.5 relation we obtain the 4.13 relation:I_{ph}

$$I = (S + S \cdot Alb) \cdot \frac{A \cdot \eta}{S_{ref}} - I_0 (e^{\frac{q \cdot V}{n \cdot k \cdot T}} - 1) \quad (4.13)$$

- Substituting the value of the photogenerated current from relation 4.9 to relation 4.5 we obtain relation 4.14:I_{ph}

$$I = S \cdot A \cdot \eta - I_0 (e^{\frac{q \cdot V}{n \cdot k \cdot T}} - 1) \quad (4.14)$$

- Substituting the value of the photogenerated current from the 4.10 relation to the 4.5 relation we obtain the 4.15 relation:I_{ph}

$$I = \int_{\lambda_{min}}^{\lambda_{max}} \Big(\big(S_\lambda \cdot SRF(\lambda) + S_\lambda \cdot Alb \cdot SRF(\lambda) \big) \cdot \eta \cdot A \Big) d\lambda - I_0 (e^{\frac{q \cdot V}{n \cdot k \cdot T}} - 1) \quad (4.15)$$

- Substituting the value of the photogenerated current from the relations 4.11 and 4.12 respectively into the relation 4.5 we obtain the relations 4.16 and 4.17 respectively:I_{ph}

$$I = (S_{dir} + Alb \cdot S_{dir}) \cdot \eta(T) \cdot A - I_0 (e^{\frac{qV}{nkT}} - 1) \quad (4.16)$$

$$I = (S + S \cdot Alb) \cdot \eta \cdot A_{pv} + K_i \cdot (T_{Pv} - T_{ref}) - I_0 (e^{\frac{qV}{nkT}} - 1) \quad (4.17)$$

4.2. DETERMINATION OF THE ALBEDO PARAMETER AS A FUNCTION OF WIND SPEED AND WAVE HEIGHT.

Albedou, defined as the ratio of reflected energy to incident energy, significantly influences the efficiency of solar energy conversion in photovoltaic systems. In this context, the albedo can be expressed by two relationships: the ratio between the power of the reflected

diffuse light and the power of the incident light (equation 4.18) or the ratio between the voltage generated by a PV exposed to diffuse light and that generated by direct sunlight (equation 4.19). [44], [45], [46], [47]

4.2.1. Description of the process.

In order to determine the Albedo as a function of wave height (m) and wind speed, the method of successive measurements was chosen using the same photovoltaic panel (the characteristics of the panel and circuit will be presented later), in different places (on the shore of places and seas) at variations in wave height and wind speed.$\left(\frac{m}{s}\right)$

For this experiment, a photovoltaic panel with a maximum power of 10Wp connected to a 32 circuit was chosen to optimize the circuit. Ω

For the greatest possible accuracy of the data, the process was repeated both on the shores of Lake Siutghiol and on the Black Sea shore, using the same photovoltaic panel for all measurements (thus eliminating possible errors).

To find out the albedo (any of the equations 4.18 and 4.19 respectively can be used:Alb)

$$Alb = \frac{V_{ref}}{V_{dir}} \quad (4.18)$$

$$Alb = 1 - \frac{\Delta V}{V_{dir}} \quad (4.19)$$

At the time of measuring the tensions, the wind speed and the height of the wave were also noted. The collected data were entered into an Excel file, after which the two mathematical models were applied (ec. 4.18; ec. 4.19).

Following the experiment it can be seen that the two hydrometeorological parameters influence the value of the albedo, so it can be said that the albedo is directly proportional to the height of the wave, respectively to the wind speed.

4.2.2. Determination of the mathematical model for Albedo as a function of wave height and wind speed.

Excel software can be used to make the mathematical model. But for the highest possible precision, the DIAdem software from National Instruments was chosen.

To determine the mathematical model of the influence of a parameter (in this case the wave height) we used the *APPROXIMATE* function in the *ANALYSIS menu*. (Figure 4.2).

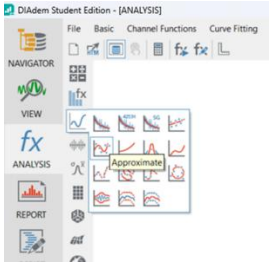

Figure 4.2 – Choosing the function for generating the mathematical model

After calling the *APPROXIMATE function,* its interface opens. The generation of the mathematical model is based on the creation of a graph in the Cartesian coordinate system XOY related to the provided data and the automatic generation of a new graph (to which a mathematical model is assigned) that overlaps with the graph of the provided data. – Figure 4.9.

- For the axis OX we have chosen as a parameter the height of the wave (m);

- For the axis I chose Albedoul.OY

After determining the axes and generating the mathematical model, *the Coefficient of Determination is* checked. For this mathematical model, the coefficient of determination is what $\mathbf{0.984}$ means that the mathematical model determined for the influence of the albedo as a function of wave height has a precision of $\mathbf{98,4\%}$.

Part II is represented by the determination of the Albedo according to the wind speed. For this stage we went through the same steps, except that we assigned the wind speed value from the database to the axis. It can be seen in figure 4.10 the generation of the mathematical model generated by the DIAdem software for the dependence of Albedo on wind speed $OX\left(\frac{m}{s}\right)$ (equation 4.21), and the value of the coefficient of determination is 0.996, i.e. the mathematical model has an accuracy of **99.6%.**

In the literature we find the *Pierson-Moskowitz law* that defines the dependence of waves on the wind. [49], [50], [51] The *Pierson-Moskowitz* model is an empirical formula that describes the energy spectrum of waves at sea under constant wind conditions over a known length of time. Equations 4.22 and 4.23 describe this pattern: [52], [53], [54]

$$S(f) = \frac{\alpha \cdot g^2}{f^5} \cdot \exp\left(-\frac{5}{4}\left(\frac{f_0}{f}\right)^4\right) \quad (4.22)$$

$$H_s = 0{,}21\ \frac{U^2}{g}\left(\frac{gX}{U^2}\right)^{0,5} \quad (4.23)$$

Since we are interested in the combined mathematical model of the Albedo, i.e. the dependence of the Albedo as a function of the wind speed and the height of the wave, we will consider that both the two disturbing elements receive a weight of 0.5 (i.e. 50%), since the height of the wave is directly proportional to the wind speed and contributes equally to the modification of the atmosphere around the mobile modules (photovoltaic system), that affect the albedo of the sea surface.

$$Alb = \frac{Alb_{val} + Alb_{vânt}}{2} \quad (4.24)$$

4.3. SIMULATION OF THE OPERATION OF A PHOTOVOLTAIC CELL AT ALBEDO VARIATIONS IN LABVIEW, USING THE MATHEMATICAL MODEL DETERMINED BY THE WAVE HEIGHT AND WIND SPEED

The introduction of simulation in PvSyst demonstrated the efficiency of mobile photovoltaic modules for powering maritime drones. Subsequently, the use of LabVIEW allowed the detailed modeling of the mathematical equations that correlate wind speed and wave height with albedo, providing an accurate simulation of electricity production.

$$I_{ph} = \left(I_{sc} + K_i \cdot \left(T - T_{ref}\right)\right) \cdot \frac{S + S \cdot Alb\ (1 - \cos\theta)}{S_{ref}} \quad (4.27)$$

$$I = I_{ph} - I_0\left(e^{\frac{qV}{nkT}} - 1\right) \quad (4.28)$$

This simulation aims to obtain the values of the current generated by the photovoltaic cells according to the determined equation.

The final equation was written in the instrumentation provided by National Instruments – Labview (Block Diagram) to provide the simulated value of current I.

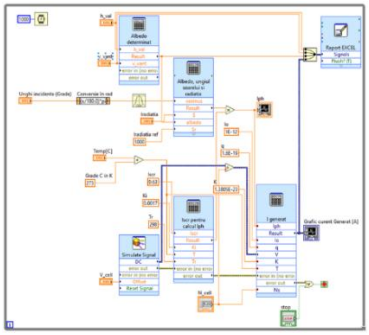

Figure 4.3 – Block diagram of the final equation written in the "Block diagram" window – LabVIEW

The mathematical model for Albedo takes into account wind speed and wave height, each with a weight of 0.5. Simulation in LabVIEW and PvSyst demonstrated the efficiency of mobile photovoltaic modules for powering maritime drones. The "Formula" blocks in LabVIEW were used to write the mathematical equations and calculate the current generated, with wave height, wind speed, sun angle, and radiation as inputs.

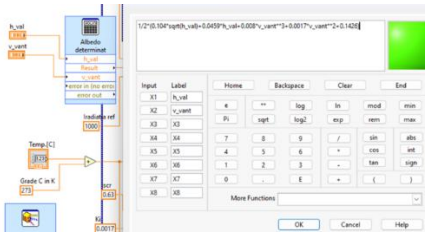

Figure 4.4 – Writing the Equation Determined in the FORMULA Block – LabVIEW

However, the radiation value of the place can be changed during the simulation.

The Formula – *Iscr block for Iph calculation* represents the first part of formula 4.27 . It was decided to divide equation 4.27 into two equations to eliminate any errors.$\left(I_{sc} + K_i \cdot \left(T - T_{ref}\right)\right)$

Simulation using PvSyst and LabVIEW showed the efficiency of mobile PV modules for powering maritime drones. The mathematical modeling of the albedo, taking into account the wind speed and the height of the wave, allowed the calculation of the current generated by the panels. Input data includes short-circuit current, panel temperature, ideality factor, and terminal voltage. The results are displayed in real time and saved in an EXCEL report.

It can be seen that the wave height and wind speed, angle of incidence and temperature can be set and changed by the user. At the same time, two windows can be seen that will display the graph of the generated current; respectively the graph of the determined mathematical model.

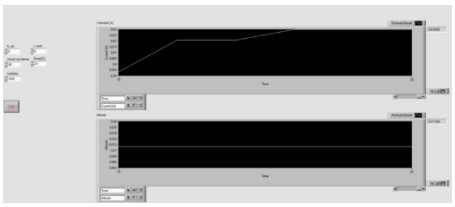

Figure 4.5 – Front panel window during simulation

Figure 4.5 shows the dependence of the current-generated (I) on the albedo (which is dependent on wind speed and wave height). It can be seen that the current graph resembles the albedo graph. For this example, an angle of incidence of , was chosen, and the simulation was started from the values of for wind speed and wave height, and the two variables were gradually

increased according to the data from the tables provided by $45\ de\ grade 0\ m/s 0\ m$ *the Maritime Hydrographic Directorate* that follows the Pierson-Moskowitz model.

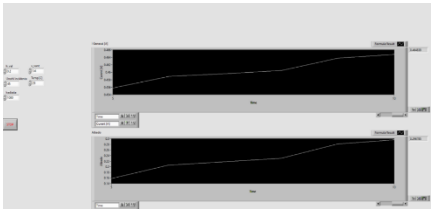

Figure 4.6 – Dependence of the current generated by the simulation

In order to validate the mathematical model, the simulation was carried out to determine the current generated by the photovoltaic panel at different hydrometeorological conditions (different values for wind speed and wave height were introduced, respecting the values provided by the Maritime Hydrographic Directorate and the National Meteorological Administration) for different angles of incidence $(10°, 20°, 30°, 40°, 45°, 50°, 60°, 70°, 80°\ şi\ 90° - cazul\ ideal)$.

4.4.ANALYSIS OF SIMULATED DATA IN DIAdem software

The data obtained from the simulations in LabVIEW were analyzed using DIAdem. The analysis highlighted the dependence of the current generated by a photovoltaic panel on the albedo defined by the mathematical model.

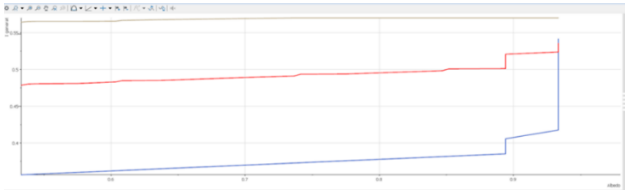

Figure 4.7 – Graph of the dependence of the current generated by the simulation of a photovoltaic panel on the albedo defined by equation 4.29 – 10Wp panel

In Figure 4.17 the graph marked in **brown** represents the value of the current generated by a photovoltaic panel, according to equation 4.30 for an **angle of incidence of 60°;** red represents the current graph defined by the same equation for an angle of incidence of **45°,** and **blue** represents the graph of the current for an angle of incidence value of . – Panel 10Wp.**30°**

Figure 4.8 shows the dependence of the current generated by a photovoltaic panel on the Albedo for all 10 angles of incidence used in the simulation (10°, 20°, 30°, 40°, 45°, 50°, 60°, 70°, 80° *şi* 90° − *cazul ideal*) for a 10 Wp panel. According to the analysis carried out by the DIAdem software, it can be seen that the Albedo defined by equation 4.29 influences the production of electricity for all cases, the variation/dependence being observed **at values lower than 60°** of the angle of incidence, because a small angle of incidence of direct radiation corresponds to a large angle formed by the photovoltaic panel with the ground, so the influence of the albedo increases significantly.

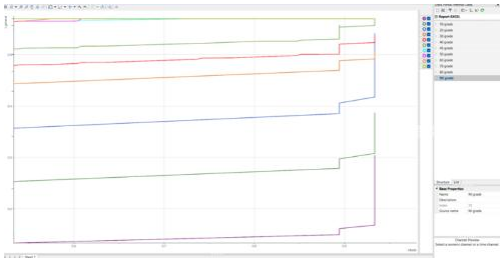

Figure 4.8 – Graphs of the currents generated for the 10 angles used in the simulation – 10Wp panel (from bottom to top the currents for the 10 angles of incidence are represented, in ascending order)

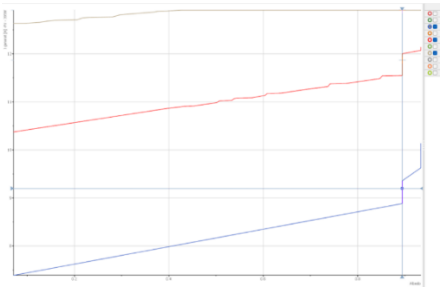

Figure 4.9 – Graph of the dependence of the current generated by a photovoltaic panel on the defined albedo – panel 395 Wp

4.5. CONCLUSIONS. CONTRIBUTIONS. PERSPECTIVES

The analysis of the influence of albedo on the performance of photovoltaic panels shows that, at angles of incidence below 60°, the reflected radiation increases the efficiency of the generated current, and at higher angles the effect is negligible. The validated mathematical model allows accurate predictions for the optimization of mobile modules intended for surface drones (USVs).

CHAPTER 5. COMPARISON OF SIMULATED DATA WITH EXPERIMENTALLY OBTAINED DATA (Validation of the determined mathematical model)

5.1. DATA ACQUISITION USING LABVIEW SOFTWARE AND USB 6008 MODULE

The data acquisition process involved the installation of a 10Wp panel on the shore of Lake Siutghiol, in *the Palazu-Mare Marine Training and Water Sports Section (SPMSN Palazu-Mare)*[1] during the period 15.03.2024 – 15.06.2024 connected to an optimal consumer for the 10Wp power. – Figure 5.1

Figure 5.1 – Photovoltaic panel with a power of 10Wp mounted on the lakeshore – SPMS Palazu-Mare

LabVIEW software was described in the previous chapter. The USB 6008 module (data acquisition plate) works as an analog-to-digital converter, with two channels for analog outputs (Analog Output), 12 channels for digital inputs and outputs (Digital Input/Output -32bit) and 8 connections for Analog Input. Connection to LabVIEW software is via a USB port. [55], [56]

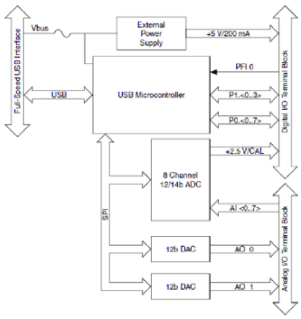

Figure 5.2 – Block diagram of the pad used for USB 6008 data acquisition [57]

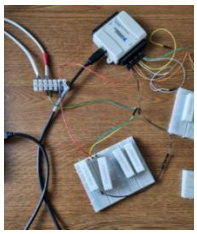

Figure 5.3 – USB 6008 plate connected to the photovoltaic panel circuit.

[1] Center dedicated to practical training for the students of the "Mircea cel Bătrân" Naval Academy in Constanta

The characteristics of the photovoltaic panel to be used for the experiment were presented in the previous chapter. Since the voltage of the panel is , and the plate used for data acquisition ($10Wp18V\,USB\ 6008$) can measure values from -to, it was necessary to create a voltage divider. In Figure 5.3 you can see that the USB 6008 is connected to such a circuit. For the power of , the voltage of and the maximum current, the optimal resistance of the circuit is , Thus, at the time of operation of the circuit, the half-value of the voltage has been applied to the terminals of the USB 6008 plate. However, LabVIEW has been programmed to display the actual voltage and current value. This will be explained later in the description of the data acquisition software.$10\,V + 10\,V10\,Wp18\,VI_{mp} = 0{,}56A32\,\Omega$

Figure 5.4 – USB 6008 card settings in the DAQ Assistant virtual component

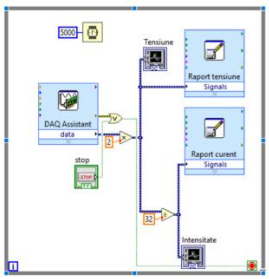

Figure 5.5 – Block scheme of the program used for real-time data acquisition

The block diagram of the algorithm for performing data acquisition performed in the *Block Diagram* window of the LabVIEW software is shown in Figure 5.5. Figure 5.6 shows the user interface (*Front Panel* window) with graphs related to measurements and real-time data acquisition.

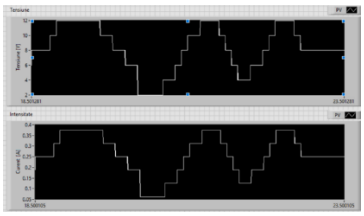

Figure 5.6 – Front Panel Window – Voltage-Current graphs displayed in real time for data acquisition

For the block diagram of the program used for real-time data acquisition, the voltage is measured at the terminals of the ceramic power resistance 15 Ω – the voltage divider – by the USB 6008 module, the measured value is doubled (using the *multiply* function with argument 2) to display the voltage value at the circuit terminals.

The generated signal is taken over and recorded in the Excel report for voltage, respectively displayed on the voltage graph; at the same time, it is processed by the *Divide* function with a value of 32 to find out the current generated by the photovoltaic panel. The current value of the photovoltaic panel is then displayed on the *Intensity* graph, respectively recorded in an Excel report.

It can be seen in figure 5.7 that for a voltage from the terminals the current generated by the photovoltaic panel has the maximum value of , according to the characteristics provided by the manufacturer. This aspect proves that the sizing of the circuit has been carried out properly.$18V0.56A$

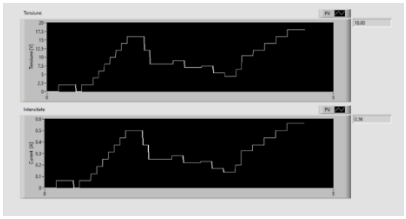

Figure 5.7 – Front Panel Window – the maximum value of the voltage and current produced by PV on the dimensioned circuit.

Figure 5.8 – Mounting the photovoltaic panel on a grassy surface

Figure 5.9 – Mounting the photovoltaic panel on a surface covered with bitumen/pitch

To determine the angle of incidence of solar radiation on the photovoltaic panel, the theoretical foundations, mathematical models and applications presented in chapter 3 (section 3.5 – *FUNDAMENTALS OF SOLAR GEOMETRY) – NOAA Solar Position Calculator, SunCalc.org, PlanetCalc.com* [58], [59], [60]

Table 5.1 – Value of the current generated for different angles of incidence [A] – panel power 10Wp – Surface: grass – (SPMSN Palazu-Mare)

Crt. No.	**Albedo Grass Value**	**Angle of incidence []°**	**I generated [A]**
1.	0,23 – 23%	10	0.1214
2.		20	0.2311
3.		30	0.3323
4.		40	0.4211
5.		45	0.4598
6.		50	0.4988
7.		60	0.5574
8.		70	0.5580
9.		80	0.5530
10.		90	0.5699

Table 5.2 – Value of the current generated for different angles of incidence [A] – panel power 10Wp – Surface: bitumen/pitch -FIM (ANMB)

Crt. No.	Albedo Grass Value	Angle of incidence []°	I generated [A]
1.	0,07 – 7%	10	0.1119
2.		20	0.2210
3.		30	0.3205
4.		40	0.3900
5.		45	0.4509
6.		50	0.4870
7.		60	0.5125
8.		70	0.5505
9.		80	0.5570
10.		90	0.5699

5.2.ANALYSIS OF DATA OBTAINED THROUGH DATA ACQUISITIONS

In order to start the analysis of the data obtained, I decided to plot the values of the currents generated by PV – 10Wp for the area covered with grass (Figure 5.10) and for the area covered with bitumen/pitch (Figure 5.11).

It can be seen from the graph that the value of the current generated by the photovoltaic (PV) panel depending on the angle of incidence of radiation on the panel, when it is on a grassy surface (albedo23%) shows an almost uniform increase to an angle of incidence of about 60 degrees, followed by a slight decrease to the value of 80 degrees, followed by an increase, reaching the maximum value at an angle of incidence of 90 degrees.

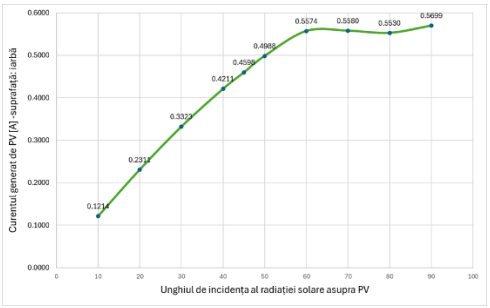

Figure 5.10 – PV Generated Current Graph for Grass Area

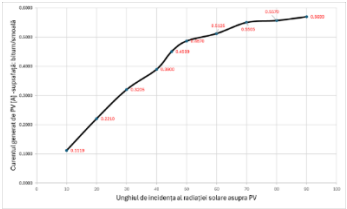

Figure 5.11 – PV Generated Current Graph for Bitumen/Pitch Area

The current generated by the photovoltaic panel mounted on the FIM roof (surface – bitumen) starts from a lower value compared to the value of the current generated by a grassy area (due to the difference in albedo), but both graphs reach similar maximum values at an angle

of incidence of 90 degrees. On the grass surface, the current peaks at about 60 degrees, and on bitumen at about 70 degrees.

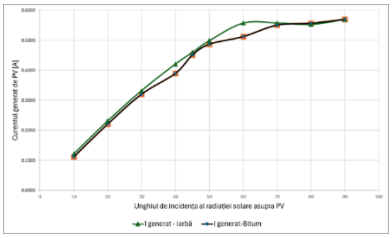

Figure 5.12 – The graph of the two currents

The values of the current generated by a photovoltaic panel at different angles of incidence of solar radiation, under certain hydrometeorological conditions presented in table 5.1, we have made the graph of the currents related to each angle of incidence – figure 5.13.

The graph of the simulated currents and the actual currents for a photovoltaic panel with a power to $10Wp$ be placed on the lakeshore can be seen in Figure 5.14, and their values are presented in Table 5.4.

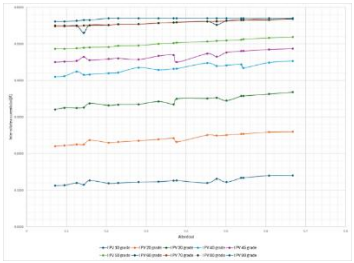

Figure 5.13 – Graph of the currents generated by the 10 Wp photovoltaic panel for different angles of incidence of solar radiation

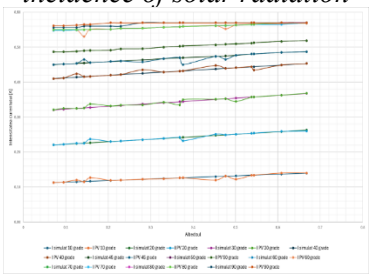

Figure 5.14 – Graph of the currents generated and simulated by/for the 10 Wp photovoltaic panel for different angles of incidence of solar radiation

For Figure 5.13 we can see that the current values for large angles of incidence of solar radiation $(60° - 90°)$ are almost identical, and the graphs overlap. At the same time, analyzing the data in table 5.1; Table 5.4 and the graphs shown in Figures 5.13 and 5.14 It can be seen that the dependence of the currents (whether simulated or real) on the value of the determined albedo is present for all angles of incidence of solar radiation on the panel, but at high values of the angle of incidence () the influence of the albedo for the production of electricity is insignificant.$60° - 90°$

For a more detailed and detailed analysis, we have chosen to separate the results presented in Figure 5.14 into two figures. The first figure (figure 5.15) shows the values of the simulated currents generated for/by the photovoltaic panel for values of the angle of incidence between and , and in the second figure (figure 5.16) I have chosen to represent the values of the simulated and generated currents for values of the angle of incidence between .$10°50°60°şi\ 90°$

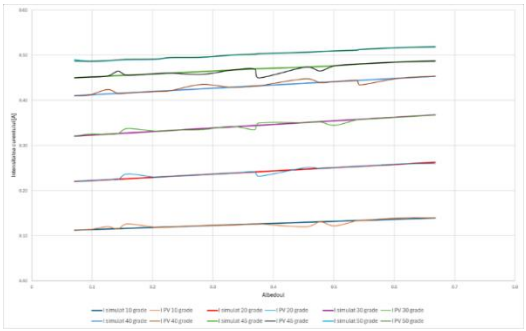

Figure 5.15 – Graph of the currents simulated/generated for/by a PV for angle values between 10° and 50°

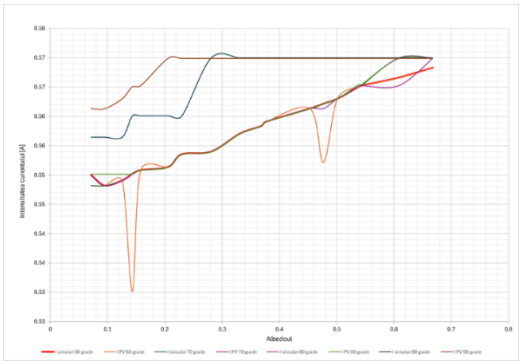

Figure 5.16 – Graph of the currents simulated/generated for/by a PV for angle values between 60° and 90°

Figure 5.16 shows the dependence of the current on the albedou for angle values between 60° and 90°. From the analysis of the two figures (5.15 and 5.16 respectively) it can be seen that the albedo (in this case the wind speed and the wave height) influences the electricity production of a photovoltaic panel at radiation incidence angles lower 80° than . In general, the value of the angle of direct radiation with a photovoltaic panel in summer has an average value over the course of a day. This aspect reinforces the idea of a forecast of electricity production in terms of mobile surface drone power supply modules, and the determined mathematical model (equation 5.2) contributes particularly to this aspect.60°

To calculate the value of the general error, we performed the arithmetic mean for each individual error, thus obtaining ***the Mean Absolute Error***, with a value of ***0.011***, and ***the Mean Relative Error***, with a value of **4.17%.** These values reflect the accuracy and precision of the determined mathematical model.

As a result of the simulations carried out, the acquisition of data and the detailed analysis, I can confidently say that the mathematical model developed, which takes into account the influence of wind speed and wave height, has been validated with remarkable accuracy. According to the predictions made in the previous chapter using the DIAdem software, the model demonstrated an accuracy of **98%,** and validation with real data indicated an accuracy of about **96%.**

The Mean Absolute Error of **0.011** and the Mean Relative Error of **4.17%** indicate a minimal deviation between the simulated and actual values, suggesting that the model can be used with confidence for predictions and applications in the context of mobile surface drone power supply modules using renewable energy sources.

Therefore, I conclude that the determined mathematical model is able to accurately predict the behavior of the analyzed system, thus satisfactorily validating itself and demonstrating considerable accuracy in both simulations and experimental measurements. This

highlights the added value of the mathematical model and justifies its use in future analyses and predictions, ensuring accuracy in the decision-making process of a drone's mission.

5.3. MOBILE POWER SUPPLY MODULES FOR SURFACE DRONES WITH RENEWABLE SOURCES

Since the determined mathematical model was validated, I decided to make a demonstrator for such a system and to mount it on the shore of Lake Siutghiol, inside *SPMSN Palazu-Mare.* Figure 5.20 shows the location where the project was assembled and carried out. [61]

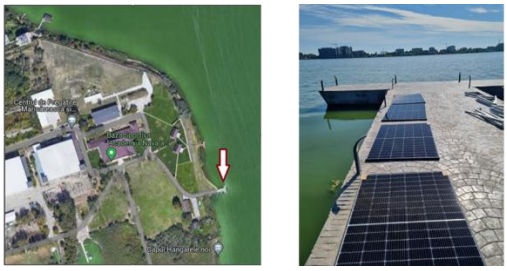

Figure 5.17 – Installation location and operation of the demonstrator "Mobile modules for power supply of surface drones

The equipment used to make the demonstrator:

- 4 photovoltaic panels – Canadian Solar 395 MS; The characteristics of the panels can be found in Table 5.8, and these can be seen in Figure 5.20;
- MPPT 150/45 (Figure 5.22) – characteristics are shown in Table 5.9.
- Mobile support for photovoltaic panels (technical drawing; sport mounted on the lakeshore – Figure 5.23);
- Lithium-iron-phosphate batteries – 25.6V, 200Ah – figure 5.24; The characteristics are shown in Table 5.10
- 48V inverter – Figure 5.24.

All materials were purchased from the funds *of the Ministry of National Defense*, within the project (for which I hold the position of project director) *"Mobile modules for the production and storage of electricity using renewable sources"* **PROJECT CODE: PSCD-I-2024-89 PLAN POSITION 89**.

Table 5.3 – Characteristics of the photovoltaic panel with a power of 395Wp

Crt. No.	**Characteristics of photovoltaic panel**	**Value**
1.	Maximum power (P_{max})	395 Wp
2.	Panel efficiency	20.2%
3.	Voltage for idling	36.6V
4.	Voltage for maximum power supply (V_{sqm})	30.6V
5.	Isc Short Circuit Current	13.77A
6.	Maximum Current (Imp)	12.91A
7.	Cell type	Single Crystal
8.	Weight	21.3kg
9.	Number of cells	108
10.	Power tolerance	0 – +10W

The Current-Voltage diagram for this type of panels according to the solar irradiation value and the temperature value of the photovoltaic panel is shown in figure 5.21. [62]

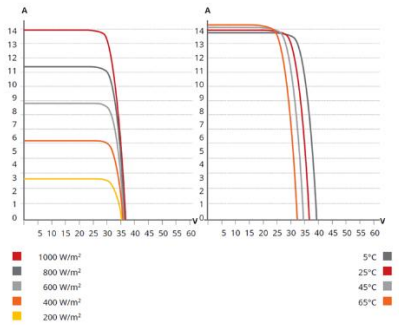

Figure 5.18 – Current Diagram – Voltage specifies the panel used to make the demonstrator [62]

Figure 5.19 – MPPT 150/45 – in the process of being connected to the circuit

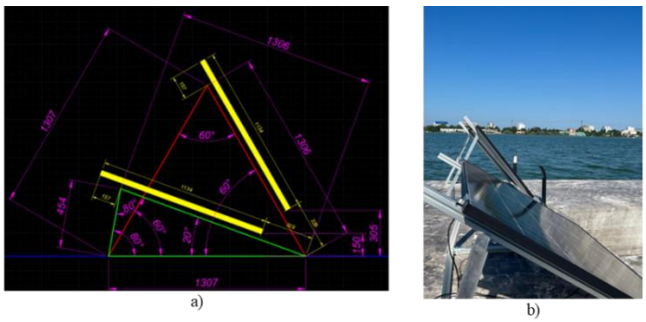

Figure 5.20 – Technical drawing of the support for the photovoltaic panels (made in AutoCAD) and the support of the panels mounted in position

From figure 5.23 it can be seen that the angle formed by PV with the ground, implicitly with the Sun's rays, can be modified depending on the hydrometeorological situation when the system is put into operation. For figure 5.23 b) we put the photovoltaic panels at different angles, just to prove the possibility of changing the angle of the panel. During the experiment, all the panels were set to the same position on the mobile support.

LiFePO4 batteries are the safest lithium ion batteries on the market. The nominal voltage of a LiFePO4 cell is 3.2V, as opposed to 2V in acid batteries, so a 12.8V battery contains 4 cells connected in series, and a 25.6V battery contains 8 cells connected in series. [63], [64]

It is not necessary for a LiFePO4 battery to be fully charged. The lifespan of such a battery improves in the case of a partial charge than a full one, which is also the great advantage over acid batteries. [63], [64]

Other advantages are the large temperature ranges in which it can operate, excellent performance in the number of cycles, low internal resistance and high efficiency, which is 92%.

Cell voltages, temperature, and error status can be monitored via Bluetooth, which is very useful for locating a potential problem, such as cell imbalance. [63], [64]

Figure 5.21 – LiFePO4 batteries and inverter used in the project

The data obtained from the simulation are presented in the previous chapter for this type of photovoltaic panel.

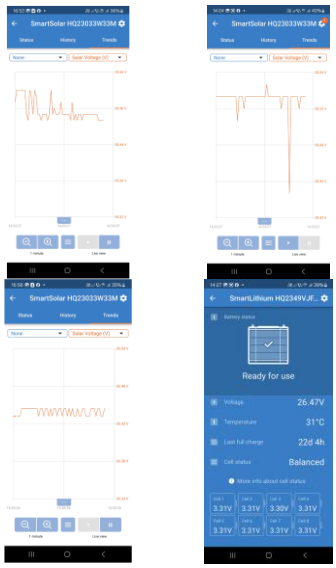

Figure 55.25 – Real-time data monitoring, via bluetooth connection of mobile phone to MPPT and batteries

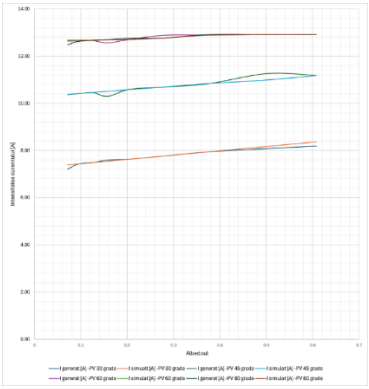

Figure 55.26 – Dependence of the current on the given albedo, according to the mathematical model defined by equation 5.1 – PV 395Wp

As a result of the simulations carried out, data acquisition and detailed analysis, I can confidently say that the developed mathematical model, which takes into account the influence of wind speed and wave height (equation 5.1), has been validated with great accuracy. According to the predictions made in the previous chapter using the DIAdem software, the model demonstrated an accuracy of **98%,** and validation with real data indicated an accuracy of about **96%** for the first experiment and an accuracy of **98.7%** for the second experiment.

The Mean Absolute Error of **0.135** and the Mean Relative Error of **1.306%** indicate a minimal discrepancy between the simulated and actual values, suggesting that the model can be used with confidence for predictions and applications in the context of mobile power supply modules for surface drones, using renewable energy sources.

Thus, I conclude that the determined mathematical model is able to accurately predict the behavior of the analyzed system, validating itself satisfactorily and demonstrating significant accuracy in both simulations and experimental measurements. This underlines the added value of the mathematical model and justifies its use in future analyses and predictions, ensuring accuracy in decision-making for surface drone missions.

CHAPTER 6. CONCLUSIONS, CONTRIBUTIONS AND PERSPECTIVES

6.1. CONCLUSIONS

Research has shown that mobile renewable energy supply modules are reliable and efficient for surface drones. The mathematical model developed to predict the albedo and current generated by photovoltaic panels has been validated with an accuracy of up to 98.7%. These modules ensure energy independence and contribute to reducing the impact on the environment.

6.2.PERSONAL CONTRIBUTIONS

The personal contributions brought by this work are varied and substantial, having both theoretical and practical impact. The first major contribution is the development of an innovative mathematical model that predicts the albedo and current generated by photovoltaic panels as a function of wind speed and wave height. This mathematical model provides an accurate and reliable method for estimating energy production under various conditions, which can optimize the operation of photovoltaic systems in maritime and river areas.

In addition to the theoretical model, we have developed and practically validated a mobile renewable energy supply module for surface drones. This involved the development, testing and optimization of an integrated energy generation and storage system, using photovoltaic panels and LiFePO4 batteries. The results obtained from the practical experiments confirmed the efficiency and reliability of this system, demonstrating the ability to operate independently of traditional energy networks.

The paper also contributes to the knowledge and understanding of the influence of weather conditions on the performance of photovoltaic panels. Through the detailed analysis of the experimental data and their simulation, we were able to provide practical recommendations for optimizing the orientation and mounting of the panels according to the specific conditions of the operating locations.

Last but not least, this work represents an important step towards the widespread adoption of renewable energy sources to power surface drones, promoting sustainability and reducing greenhouse gas emissions.

6.3.DEVELOPMENT PROSPECTS

The prospect of the future development of this research is extremely promising and opens up numerous opportunities for expansion and innovation. A key area of development is the extension of the applicability of mobile renewable energy supply modules to other types of drones and maritime applications. This could include, for example, small hydrographic research vessels or monitoring equipment.

In addition, the integration of advanced energy storage technologies, such as next-generation batteries and supercapacitors, can greatly improve the efficiency and storage capacity of these modules. Also, the development of optimization algorithms for energy management could maximize the performance and reliability of systems under various conditions.

Another important direction is to deepen climate studies to better understand the influence of extreme weather conditions on the performance of photovoltaic panels. These

studies can lead to the adaptation of mathematical models and mounting strategies to ensure optimal performance in any conditions.

A relevant addition to the development perspective would be the implementation of a hybrid system, combining photovoltaic panels with a small wind turbine. This system would allow continuous power generation, even in adverse weather conditions for solar energy, thus maximizing the autonomy and efficiency of the mobile modules. The integration of the two renewables would ensure greater operational flexibility and adaptability in various maritime environments, while providing a sustainable model for the use of renewable energy in maritime and coastal applications.

There is also significant potential for interdisciplinary collaboration and the development of pilot projects in cooperation with industry and research institutions. These projects could aim at the large-scale testing and deployment of mobile modules in different environments and applications, providing valuable data for the continuous improvement of technologies.

In conclusion, the research and innovations presented in this paper pave the way for new opportunities and developments in the field of renewable energy and surface drones.

The implementation of these technologies can significantly contribute to a sustainable future and to the reduction of negative environmental impact.

BIBLIOGRAPHY

[1] "Tesla's Inventions 3D – Nikola Tesla Museum." Accessed: Jun 17, 2024. [Online]. Available: https://tesla-museum.org/en/nikola-tesla-2/teslas-inventions-3d/

[2] "Nikola Tesla and the Wireless World: The Invention of Remote Control - The Bowery Boys: New York City History." Accessed: Jun 17, 2024. [Online]. Available: https://www.boweryboyshistory.com/2017/03/nikola-tesla-wireless-world-invention-remote-control.html

[3] R. Chen, C. Yang, S. Han, and J. Zheng, "Dynamic path planning of USV with towed safety boundary in complex ocean environment," *Proceedings of the 33rd Chinese Control and Decision Conference, CCDC 2021*, pp. 71–76, 2021, doi: 10.1109/CCDC52312.2021.9602804.

[4] J. Li and G. Zhang, "Dynamic surface control for path following of the USV-UAV with time-varying disturbances," *2022 34th Chinese Control and Decision Conference (CCDC)*, pp. 3115–3120, Aug. 2022, doi: 10.1109/CCDC55256.2022.10033603.

[5] F. M. Raimondi, M. Trapanese, V. Franzitta, and V. Di Dio, "Identification of the inertial model for innovative semi-immergible USV (SI-USV) drone for marine and lakes operations," *OCEANS 2015 - MTS/IEEE Washington*, Feb. 2016, doi:10.23919/OCEANS.2015.7404555.

[6] Z. Liu, Y. Zhang, X. Yu, and C. Yuan, "Unmanned surface vehicles: An overview of developments and challenges," *Year Rev Control*, vol. 41, pp. 71–93, 2016, doi: 10.1016/J.ARCONTROL.2016.04.018.

[7] M. Breivik, V. E. Hovstein, and T. I. Fossen, "Straight-line target tracking for unmanned surface vehicles," *Modeling, Identification and Control*, vol. 29, no. 4, pp. 131–149, 2008, doi: 10.4173/MIC.2008.4.2.

[8] **N.-S. Popa**, C. Popa, V. Mocanu, and L.-M. POPA, "State of the Art in Battery Technology: Innovations and Advancements," *Journal of Marine Technology and Environment*, pp. 81–85, 2023.

[9] O. Cristea, N.-S. Popa, M.-G. Manea, and C. Popa, "About the Automation of an Autonomous Sail-propelled Search Drone," *Engineering, Technology & Applied Science Research*, vol. 13, no. 6, pp. 12334–12341, 2023.

[10] **N.-S. Popa**, A. POPESCU, V. Mocanu, M. TĂRHOACĂ, and C. Popa, "Producing electricity on board a ship in motion or stationary using photovoltaic panels.," *Technium*, vol. 14, 2023.

[11] V. MOCANU, M. O. POPESCU, and N.-S. P. VasileDOBREF, "OPTIMIZATION OF COIL INDUCTANCE EQUATIONS USED IN WIRELESS POWER TRANSFER FOR DRONE CHARGING".

[12] **N.-S. Popa**, M.-O. Popescu, and V. Mocanu, "State of the Art-Drones/Surface Platforms and Green Energy," in *IOP Conference Series: Earth and Environmental Science*, IOP Publishing, 2023, p. 012004.

[13] IRENA *Future of solar photovoltaic: Deployment, investment, technology, grid integration and socio-economic aspects (A Global Energy Transformation: paper)*, vol. November. 2019. [Online]. Available: https://www.irena.org/-/media/Files/IRENA/Agency/Publication/2019/Oct/IRENA_Future_of_wind_2019.pdf

[14] **N.-S. Popa** and C. Popa, "Li-Ion battery discharge study," *Scientific Bulletin" Mircea cel Batran" Naval Academy*, vol. 24, no. 2, pp. 1–8, 2021.

[15] A. Sciences, "Off-grid Solar Power Systems in Rural Areas," 2017.

[16] A. Zablocki, *Energy Storage. Fundamentals, MAterials and Apps*, vol. 2040, no. February. 2019.

[17] M. R. Patel, "Wind and solar power systems: Design, analysis, and operation, second edition," *Wind and Solar Power Systems: Design, Analysis, and Operation, Second Edition*, pp. 1–448, 2005, doi: 10.2134/JEQ2006.0001BR.

[18] T. Song, L. Ottoson, J. Gallon, D. J. Friedman, and N. Kopidakis, "Reliable Power Rating of Perovskite PV Modules," *Conference Record of the IEEE Photovoltaic Specialists Conference*, pp. 367–371, 2021, doi: 10.1109/PVSC43889.2021.9518841.

[19] P. V. Rosu, A. T. Plesca, G. Gabor, and G. Chiriac, "Optimizing the Operation of Photovoltaic Panel Systems," *EPE 2020 - Proceedings of the 2020 11th International Conference and Exposition on Electrical And Power Engineering*no. Epe, pp. 318–321, 2020, doi: 10.1109/EPE50722.2020.9305534.

[20] A. Mallama, B. Krobusek, and H. Pavlov, "Comprehensive wide-band magnitudes and albedos for the planets, with applications to exo-planets and Planet Nine," *Icarus*, vol. 282, pp. 19–33, Jan. 2017, doi: 10.1016/j.icarus.2016.09.023.

[21] A. K. Betts and J. H. Ball, "Albedo over the boreal forest," *J Geophys Res*, vol. 102, no. D24, pp. 28, 901–28, 910, Dec. 1997, doi: 10.1029/96JD03876.

[22] C. T. Ruhland and J. A. Niere, "The effects of surface albedo and initial lignin concentration on photodegradation of two varieties of Sorghum bicolor litter," *Ski Rep*, vol. 9, no. 1, p. 18748, Dec. 2019, doi: 10.1038/s41598-019-55272-x.
[23] "National Energy System - Transelectrica." Accessed: Jan. 22, 2023. [Online]. Available: https://www.transelectrica.ro/web/tel/sistemul-energetic-national
[24] Y. Hou, K. Kang, Y. Xiong, X. Liang, and L. Su, "Uncertainty optimisation design of USV based on the Six Sigma method," *Ocean Engineering*, vol. 200, Mar. 2020, doi: 10.1016/j.oceaneng.2020.107045.
[25] M. Toll, "DIY Lithium Batteries How to Build Your Own Battery Packs Written by Micah Toll," 2017.
[26] V. N. Duy and H. M. Kim, "Review on the hybrid-electric propulsion system and renewables and energy storage for unmanned aerial vehicles," *Int J Electrochem Sci*, vol. 15, pp. 5296–5319, 2020, doi: 10.20964/2020.06.13.
[27] M. Toll, "DIY Lithium Batteries How to Build Your Own Battery Packs Written by Micah Toll," 2017.
[28] "Photovoltaic Cells by Juan Carlos Ferrer | PPT." Accessed: Jun. 24, 2024. [Online]. Available: https://www.slideshare.net/slideshow/clulas-fotovoltaicas-por-juan-carlos-ferrer/21318142#5
[29] P. Vanderhulst, H. Lanser, P. Bergmeyer, and R. Albers, "Solar energy: small scale applications in developing countries," *Int Food J*, vol. 8, no. c, pp. 138–145, 1990.
[30] S. Sumathi, L. Ashok Kumar, and P. Surekha, *Solar PV and Wind Energy Conversion Systems: Introduction to Theory, Modeling with MATLAB/SIMULINK, and the Role of Soft Computing Techniques*. 2015. [Online]. Available: http://link.springer.com/10.1007/978-3-319-14941-7
[31] O. Cristea, "Testing of PV module efficiency in naval conditions," *2013 - 8th International Symposium on Advanced Topics in Electrical Engineering, ATEE 2013*, 2013, doi:10.1109/ATEE.2013.6563534.
[32] P. Carolyn. Roos, "Solar Electric System Design, Operation and Installation," *Washington State University Extension Energy Program*no. October, p. 35, 2009, [Online]. Available: www.energy.wsu.edu
[33] Anon., "Fundamental Properties of Solar Cells, Principles and Varieties of Solar Energy," no. Phys 4400, p. 13, 2012.
[34] "Installation of photovoltaic systems", [Online]. Available: www.pvtrin.eu
[35] "PVsyst – Photovoltaic software." Accessed: Nov. 20, 2023. [Online]. Available: https://www.pvsyst.com/
[36] M. Flores-Nicolás, M. M. Reyes, F. O. S. Hernández, and C. P. Martínez, "Implementation of the new multidisciplinary gradual model for the development of a didactic sequence under Blum's modeling cycle approach in descriptive statistics," *2021 Mexican International Conference on Computer Science, ENC 2021*, Aug. 2021, doi: 10.1109/ENC53357.2021.9534766.
[37] M. K. Da Silva, D. I. Narvaez, K. B. De Melo, and M. G. Villalva, "Comparative analysis of transposition models applied to photovoltaic systems using meteonorm and NASA SSE databases," *2018 13th IEEE International Conference on Industry Applications, INDUSCON 2018 - Proceedings*, pp. 237–241, Jul. 2019, doi: 10.1109/INDUSCON.2018.8627354.
[38] V. A. Martinez Lopez, G. van Urk, P. J. F. Doodkorte, M. Zeman, O. Isabella, and H. Ziar, "Using sky-classification to improve the short-term prediction of irradiance with sky images and convolutional neural networks," *Solar Energy*, vol. 269, Feb. 2024, doi: 10.1016/j.solener.2024.112320.
[39] D. Yang *et al.*, "Regime-dependent 1-min irradiance separation model with climatology clustering," *Renewable and Sustainable Energy Reviews*, vol. 189, Jan. 2024, doi: 10.1016/j.rser.2023.113992.
[40] M. J. Marín, D. Serrano, M. P. Utrillas, M. Núñez, and J. A. Martínez-Lozano, "Effective cloud optical depth and enhancement effects for broken liquid water clouds in Valencia (Spain)," *Atmos Nothing*, vol. 195, pp. 1–8, Oct. 2017, doi: 10.1016/j.atmosres.2017.05.008.
[41] C. A. Gueymard, "Cloud and albedo enhancement impacts on solar irradiance using high-frequency measurements from thermopile and photodiode radiometers. Part 1: Impacts on global horizontal irradiance," *Solar Energy*, vol. 153, pp. 755–765, Sep. 2017, doi: 10.1016/J.SOLENER.2017.05.004.
[42] G. R. Timilsina, L. Kurdgelashvili, P. A. N. The, and W. Bank, "A Review of Solar Energy Markets, Economics and Policies," 2011. [Online]. Available: http://econ.worldbank.org.
[43] *Solar energy: small-scale applications in developing countries.* TOOL Foundation, 1990.
[44] Y. Li *et al.*, "Interannual variability of the surface summertime eastward jet in the South China Sea," *J Geophys Res Oceans*, vol. 119, no. 10, pp. 7205–7228, Oct. 2014, doi: 10.1002/2014JC010206.
[45] W. Munk and C. Cox, "Measurement of the Roughness of the Sea Surface from Photographs of the Sun's Glitter," *JOSA, Vol. 44, Issue 11, pp. 838-850*, vol. 44, no. 11, pp. 838–850, Nov. 1954, doi: 10.1364/JOSA.44.000838.

[46] F. M. Bréon and N. Henriot, "Spaceborne observations of ocean glint reflectance and modeling of wave slope distributions," *J Geophys Res Oceans*, vol. 111, no. C6, p. 6005, Jun. 2006, doi: 10.1029/2005JC003343.

[47] W. S. Broecker *et al.*, "How much deep water is formed in the Southern Ocean?," *J Geophys Res Oceans*, vol. 103, no. C8, pp. 15833–15843, Jul. 1998, doi: 10.1002/(ISSN)2156-2202C.

[48] "What Is DIAdem? - NEITHER." Accessed: Apr 07, 2024. [Online]. Available: https://www.ni.com/en/shop/data-acquisition-and-control/application-software-for-data-acquisition-and-control-category/what-is-diadem.html

[49] "Pierson-Moskowitz Spectrum - an overview | ScienceDirect Topics." Accessed: Apr 08, 2024. [Online]. Available: https://www.sciencedirect.com/topics/engineering/pierson-moskowitz-spectrum

[50] Y. Bai and W.-L. Jin, "Wave Loads for Ship Design and Classification," *Marine Structural Design*, pp. 73–93, 2016, doi: 10.1016/B978-0-08-099997-5.00005-8.

[51] G. E. Hearn and A. V Metcalfe, "Motions of moored structures in a seaway," *Spectral Analysis in Engineering*, pp. 208–232, 1995, doi: 10.1016/B978-034063171-3/50011-7.

[52] M. Karimirad and Z. Jiang, "2.08 - Mechanical-Dynamic Loads," *Comprehensive Renewable Energy, Second Edition: Volume 1-9*, vol. 1–2, pp. 194–225, Jan. 2022, doi: 10.1016/B978-0-12-819727-1.00075-3.

[53] "3 Ocean waves," *Elsevier Ocean Engineering Series*, vol. 4, no. C, pp. 43–122, 2001, doi: 10.1016/S1571-9952(01)80005-2.

[54] M. A. Hanif, F. Nadeem, R. Tariq, and U. Rashid, "Power generation by ocean energy," *Renewable and Alternative Energy Resources*, pp. 359–430, 2022, doi: 10.1016/B978-0-12-818150-8.00002-2.

[55] "USB-6008 National Instruments Multifunction I/O Device | Apex Waves." Accessed: Nov. 06, 2022. [Online]. Available: https://www.apexwaves.com/modular-systems/national-instruments/usb-multifunction-devices/USB-6008?matchtype=e&network=g&device=c&keyword=usb-6008&campaign=17954270381&adgroup=138410153943&gclid=CjwKCAjwtp2bBhAGEiwAOZZTuB_EELMon7Xxbo05rAxlY9t-71yUGYYKN5C2_GpxILU007nnoHh-mxoC1QEQAvD_BwE

[56] P. By ALLDATASHEETCOM, "Low-Cost, Bus-Powered Multifunction DAQ for USB-12-or 14-Bit, up to 48 kS/s, 8 Analog Inputs."

[57] "USB-6008 block diagram [5] | Download Scientific Diagram." Accessed: Jun. 07, 2024. [Online]. Available: https://www.researchgate.net/figure/USB-6008-block-diagram-5_fig4_341090594

[58] "Solar Position Calculator." Accessed: Jun. 24, 2024. [Online]. Available: https://gml.noaa.gov/grad/solcalc/azel.html

[59] "SunCalc - sunrise, sunset, shadow length, solar eclipse, sun position, sun phase, sun height, sun calculator, sun movement, map, sunlight phases, elevation, Photovoltaic system, Photovoltaic." Accessed: Jun. 24, 2024. [Online]. Available: https://www.suncalc.org/#/43.9947,28.6491,14/2024.06.14/16:29/1/1

[60] "Online calculator: Sun position." Accessed: Jun. 24, 2024. [Online]. Available: https://planetcalc.com/318/

[61] "Google Maps." Accessed: Jun 10, 2024. [Online]. Available: https://www.google.com/maps/@44.2314154,28.6113685,670m/data=!3m1!1e3?entry=ttu

[62] C. Solar Co Ltd, "PARTNER SECTION ENGINEERING DRAWING (mm) Rear View Mounting Hole CS6R-405MS/I-V CURVES." [Online]. Available: www.csisolar.com,

[63] "Lithium LiFePo4 25.6V 200Ah Smart Photovoltaic Battery, Victron - SolarTech Photovoltaic." Accessed: Jun 10, 2024. [Online]. Available: https://solartech.ro/acumulator-fotovoltaice-litiu-lifepo4-25-6v-200ah-smart-victron-copiaza/?utm_source=Google%20Shopping&utm_campaign=google_test&utm_medium=cpc&utm_term=13658&gad_source=1&gclid=CjwKCAjwyJqzBhBaEiwAWDRJVEbvA1dtXRnkgsUAL3nrWV6KriM1h8jIH6reEe1ZVOjtmmjima2OxxoC5GIQAvD_BwE

[64] "Datasheet-12,8-&-25,6-Volt-lithium-iron-phosphate-batteries-Smart-RO".